This is the accepted version of the manuscript that was published in
Wu, K., Benchimol, E., Baksi, A. *et al.* Non-statistical assembly of multicomponent [Pd2ABCD] cages. *Nat. Chem.* **16**, 584–591 (2024). https://doi.org/10.1038/s41557-023-01415-7

Nonstatistical Assembly of Multicomponent [Pd$_2$ABCD] Cages

Kai Wu,[1,2] Elie Benchimol,[1] Ananya Baksi[1,3] and Guido H. Clever[1]*

[1]Department of Chemistry and Chemical Biology, TU Dortmund University, Otto-Hahn-Str. 6, 44227 Dortmund, Germany.

[2]Present address: MOE Laboratory of Bioinorganic and Synthetic Chemistry, LIFM, IGCME, School of Chemistry, Sun Yat-Sen University, Guangzhou 510275, China.

[3]Present address: Department of Chemistry, Jadavpur University, Kolkata-700032, West Bengal, India.

*e-mail: guido.clever@tu-dortmund.de

ABSTRACT: Self-assembled hosts, inspired by biological receptors and catalysts, show potential for sustainable synthesis, energy conversion and medicine. Implementing multiple functionalities in the form of distinguishable building blocks, however, is difficult without risking narcissistic self-sorting or statistical mess. Here, we report a systematic series of integratively self-assembled heteroleptic cages in which two square-planar Pd^{II} cations are bridged by four different bis-pyridyl ligands **A**, **B**, **C** and **D** via synergistic effects to exclusively form a single isomer — the lantern-shaped cage [Pd$_2$**ABCD**]. This self-sorting goal — forming just one out of 55 possible structures — is reached under full thermodynamic control and can be realized progressively (by combining progenitors such as [Pd$_2$**A**$_2$**C**$_2$] with [Pd$_2$**B**$_2$**D**$_2$]), directly from ligands and Pd^{II} cations, or by mixing all four corresponding homoleptic cages. The rational design of complex multicomponent assemblies that enables the incorporation of chemical moieties in a modular approach will advance their potential applications in functional nanosystems.

Biological systems have evolved precisely shaped nano-confinements of low symmetry for the selective recognition of C_1-symmetric substrates and their catalytic conversion[1]. Enzymes utilize folded peptide chains as scaffolds to position and structurally support active elements such as binding sites and catalytic centers around defined cavities[2]. Inspired by this, synthetic chemists have developed supramolecular systems that resemble their biological paradigms, including purely organic[3] and metal-mediated assemblies[4–6], to achieve molecular recognition and separation[7], reactive species stabilization[6,8], and confined catalysis[9]. In case of metallosupramolecular assemblies, further applicability can be achieved by using ligands equipped with dedicated functional units such as chiral groups[10], luminophores[11], redox centers[12,13] or photoswitches[14,15]. Nevertheless, a majority of reported examples consist of only one type of organic ligand per assembly, hence they are homoleptic, often have rather isotropic cavities, and high symmetries derived from Platonic or Archimedean solids[16,17]. This may limit their application potential in advanced settings that require synergistic interplay of different

ligand constituents, e.g. between recognition sites, catalytic moieties and chiral modulators. Multifunctional assemblies with contribution from two different components are still in their infancy, e.g. systems featuring intraassembly chirality transfer[18], charge-transfer[19], and cooperative catalysis[20–22]. In only few of the most complicated self-assembled systems reported to date, more than two differentiable functionalities, situated on separate components, are involved[20,23,24].

Inspired by seminal investigations of Lehn[25], Sauvage[26], Fujita[27], Stang[28] and others[29], recent developments in the area of metallosupramolecular assembly have enabled the rational and clean combination of multiple building blocks in a non-statistical fashion. Integrative self-sorting strategies have overcome entropic control and prevent the formation of statistical mixtures[30,31]. These include shape-complementary assembly (SCA)[32–36], charge-separation[20,28], templating effects[27,37], coordination sphere engineering (CSE)[38,39], the use of non-symmetric ligands[40,41], backbone steric hindrance[42], and multidentate donor environments[43].

Within the popular class of Pd^{II}-mediated structures, the lowest nuclearity, hence most simple, assembly with an accessible cavity is a lantern-shaped $[Pd_2L_4]$ cage in which two square-planar cations are connected by four banana-shaped bis-monodentate pyridyl ligands. While most of the numerous reported examples are composed of a single type of ligand per assembly, recent studies by Crowley[39], Hooley[44], Zhang[45] and us[33] have shown that a proper choice of ligands allows to rationally combine two or – and this only via kinetic control[45] – even three, different ligands without creating statistical mixtures. Both from an entropic as well as chemical design point of view, the difficulty to achieve integrative self-sorting under thermodynamic control steeply increases when all four ligands that ought to be combined are different.

Results and discussion

In theory, without rational control, a supramolecular system consisting of four distinguishable bis-monodentate ligands **A**, **B**, **C**, and **D**, equally and independently able to coordinate to two square-planar Pd^{II} nodes, will lead to the formation of 55 different species (Supplementary Scheme 1), ranging from the simplest lantern-shaped homoleptic cages, e.g. $[Pd_2\mathbf{A}_4]^{4+}$, to multicomponent cages, e.g. $[Pd_2\mathbf{ABCD}]^{4+}$, with the highest complexity.

Here we report the systematic construction of a family of non-statistically assembled heteroleptic cages in which two square-planar Pd^{II} cations are bridged by up to four chemically different ligands (Fig. 1). Ligand shape-complementarity, together with stabilizing C-H···π

interactions and strain effects allow to reach this extreme level of integrative self-sorting. The increase in complexity can be realized either progressively, by successive cage-to-cage transformations from homo- via two- and three-component heteroleptic cages, or directly by mixing either all ligands with Pd^{II} or all four homoleptic cages. In the following, we compare these routes with the help of a comprehensive set of NMR and mass spectrometry results as well as nine single crystal X-ray structures of heteroleptic cages.

Heteroleptic cages with two different ligands

Recently, we reported that combining shape-complementary bis-monodentate ligands $\mathbf{B^0}$ and **C** with square-planar Pd^{II} cations in acetonitrile yields heteroleptic cage $[Pd_2\mathbf{B^0}_2\mathbf{C}_2]^{4+}$ through the SCA approach as single thermodynamic product[46]. Here, by replacing ligand **C** with its fluorenone-based analogue **D**, cage $[Pd_2\mathbf{B^0}_2\mathbf{D}_2]^{4+}$ was obtained exclusively as proven by 2D NMR and high-resolution electrospray ionization mass spectrometry (HR-ESI-MS; Supplementary Figs. 92-98). Similarly, by replacing ligand $\mathbf{B^0}$ with **B**, heteroleptic cages $[Pd_2\mathbf{B}_2\mathbf{C}_2]^{4+}$ and $[Pd_2\mathbf{B}_2\mathbf{D}_2]^{4+}$ were obtained selectively (Supplementary Figs. 31-44). To achieve the introduction of three or four different ligands, further shape-complementary ligand pairs needed to be explored. We previously reported that curved ligand **A** forms cage $[Pd_2\mathbf{A}_4]^{4+}$, suitable for fullerene encapsulation[38]. Here we show that **A** is also able to cleanly form heteroleptic cages $[Pd_2\mathbf{A}_2\mathbf{C}_2]^{4+}$ and $[Pd_2\mathbf{A}_2\mathbf{D}_2]^{4+}$ together with ligands **C** and **D**, respectively. NMR, ESI-MS and single crystal X-ray experiments of *trans*-$[Pd_2\mathbf{A}_2\mathbf{B}_2]^{4+}$ (Fig. 2a) clearly demonstrated the suitability of these ligand combinations for clean heteroleptic cage formation, both in solution and the solid state (Supplementary Figs. 52-63).

Heteroleptic cages with three different ligands

Next, we aimed at further increasing the system's structural complexity by introducing a third differentiable ligand. Therefore, we carefully inspected ligands **C** and **D** – both complements of ligands **A** or **B** – and realized that although they share a similar backbone and the same pyridyl donors, their electronic properties are distinguishable. Ligand **C** comprises a central dimethyl group, a potential C-H···π donor, while ligand **D**, presenting an unobstructed π-surface, could act as a complementary acceptor. We thus suspected that the assembly of ligands **A**, **C**, and **D** with Pd^{II} leads to a preferential interaction between neighboring ligands **C** and **D** through integrative self-sorting[42], energetically surpassing the interaction between pairs of **C** or **D** in the competing assemblies $[Pd_2\mathbf{A}_2\mathbf{C}_2]^{4+}$ or $[Pd_2\mathbf{A}_2\mathbf{D}_2]^{4+}$. Indeed, the assembly of ligands **A**, **C**, and **D** with Pd^{II} in a 2:1:1:2 ratio in CD_3CN at 80 °C resulted in a well-resolved ^1H NMR spectrum (Fig. 3). ^1H DOSY confirmed the formation of a single species, with a

diffusion coefficient of 6.32×10^{-10} m^2 s^{-1}, corresponding to a hydrodynamic radius of 1.0 nm (Supplementary Fig. 69), consistent with the size of a heteroleptic cage $[Pd_2\mathbf{A}_2\mathbf{CD}]^{4+}$. The structure of cage $[Pd_2\mathbf{A}_2\mathbf{CD}]^{4+}$ was confirmed by X-ray diffraction analysis (Fig. 2b). Noteworthy, both ligands **A** were found to be direct neighbors, unlike the *trans*-arrangement seen in cage $[Pd_2\mathbf{A}_2\mathbf{B}_2]^{4+}$ (compare Figs. 2a and b). As shown earlier, also ligand **B** can be a shape-complementary partner to both ligands **C** and **D**. Indeed, integrative self-sorting also proceeded when combining ligands **B**, **C**, **D** with Pd^{II}, yielding cage $[Pd_2\mathbf{B}_2\mathbf{CD}]^{4+}$ with a similar NMR pattern and characteristic HR-ESI-MS spectrum (Supplementary Figs. 45-51).

Next, we kept shorter ligands **C** and **D** as identical pairs and mixed these with **A** and **B** aimed at the formation of cages $[Pd_2\mathbf{ABC}_2]^{4+}$ and $[Pd_2\mathbf{ABD}_2]^{4+}$, respectively. Pleasingly, the mixture of ligands **A**, **B**, **C** and Pd^{II} in stoichiometric ratio yielded a well-resolved NMR spectrum. Again, HR-ESI-MS confirmed clean formation of a cage with formula $[2Pd^{II}+\mathbf{A}+\mathbf{B}+2\mathbf{C}]^{4+}$ (Supplementary Figs. 71-77). Now, the two ligands **C** have different chemical environments and the correlation between their protons H7 and H7' rules out the formation of a *trans*-configured cage (Supplementary Fig. 75). Likewise, the formation of cage $[Pd_2\mathbf{ABD}_2]^{4+}$ was achieved by replacing ligand **C** with **D** under otherwise same conditions (Supplementary Figs. 78-84).

Heteroleptic cages with four different ligands

Eventually, we tackled the most challenging self-assembly, involving the simultaneous incorporation of four chemically different ligands. Remarkably, the combination of ligands **A**, **B**, **C**, and **D** with Pd^{II} in a 1:1:1:1:2 ratio in CD_3CN at 80 °C resulted in a complex, yet well-resolved, NMR spectrum showing four sets of signals originating from ligands **A**, **B**, **C**, and **D** with 1:1:1:1 integration ratio (Fig. 3a). ^{1}H DOSY confirmed that all peaks belong to the same diffusion coefficient of 6.38×10^{-10} m^2 s^{-1} (Supplementary Fig. 90). The exclusive formation of a heteroleptic cage with sum formula $[2Pd^{II}+\mathbf{A}+\mathbf{B}+\mathbf{C}+\mathbf{D}]^{4+}$ was verified by HR-ESI-MS (Fig. 2c, Supplementary Fig. 91).

By arranging four different ligands circularly around two metal nodes, three configurational isomers with C_s-symmetry are possible (Fig. 4b). While mass spectrometry reveals the stoichiometry, it cannot answer which isomer is formed. From the results discussed earlier, we concluded that longer ligands **A** and **B** should be positioned in a *cis*-relationship. The same is true for shorter ligands **C** and **D** to allow for attractive interligand contacts and maximize the shape-complementary fit. Thus, a tentative $[Pd_2\mathbf{ADBC}]^{4+}$ isomer, carrying **A** and **B** in a *trans*-relationship, could be ruled out, leaving only two possible isomers, i.e. $[Pd_2\mathbf{ABCD}]^{4+}$ and $[Pd_2\mathbf{ABDC}]^{4+}$. NOESY correlations between protons H7 of ligands **A** and **B** and protons H7

of ligands **C** and **D** also support either of the latter two isomers (Fig. 3b), however, no correlations could be found between protons H7 of ligands **A** and **C** or **D** to distinguish these two isomers. Single crystals were obtained by vapor diffusion of benzene to the cage solution in CD_3CN. Structural analysis confirmed the formation of the $[Pd_2\mathbf{ABCD}]^{4+}$ isomer (Fig. 1).

Next, we investigated the rationale leading to this remarkable selectivity. The dihedral angle between the $Pd(Py)_4$ planes in the structure was measured to be 21°, indicating that shape-complementarity plays an important role (Fig. 4b). Although the selective formation of both cages $[Pd_2\mathbf{ABC}_2]^{4+}$ and $[Pd_2\mathbf{ABD}_2]^{4+}$ was found to be possible from the respective three-ligand mixtures, the clean assembly of cage $[Pd_2\mathbf{ABCD}]^{4+}$ from all four ligands indicates a significant interligand contact between ligands **C** and **D**. The structure reveals that both of the geminal methyl groups on ligand **C** point to the π-surface of ligand **D**, forming C-H···π interactions with average distances of 2.9–3.1 Å, which is even closer than found in the X-ray structure of $[Pd_2\mathbf{A}_2\mathbf{CD}]^{4+}$ in which only one methyl group interacts with the neighboring ligand (compare Figs. 1 and 2b).

To probe the importance of the dimethyl C-H···π donor motif of **C**, we performed a series of control experiments by keeping ligands **A**, **B** and **D** the same but modifying the central part of ligand **C** (Fig. 4a). First, ligand $\mathbf{D^1}$, featuring an NH moiety, was combined with ligands **A**, **B**, **D**, resulting in a convoluted NMR spectrum containing more than four species (Supplementary Figs. 126-127). Then, similar ligand $\mathbf{D^2}$ with a $N\text{-}CH_3$ group was employed, offering only one methyl group to form C-H···π interactions. This again resulted in a complicated NMR spectrum, indicating a lack of self-sorting, although the MS spectrum showed cage $[Pd_2\mathbf{ABD^2D}]^{4+}$ as the major species (Supplementary Figs. 128-129). We managed to selectively crystallize cage $[Pd_2\mathbf{ABD^2D}]^{4+}$ from this mixture (Supplementary Fig. 299). Although its structure clearly showed a C-H···π interaction from the methyl group of $\mathbf{D^2}$ to the π-surface of **D**, we suppose that its strength is not sufficient to promote selective sorting in solution. The methyl group in $\mathbf{D^2}$ sits in plane with the ligand backbone, while the two methyl groups of **C** protrude sideways from an sp^3-carbon (Supplementary Figs. 125). To rule out an orientation effect on the strength of the C-H···π interaction, we designed ligand $\mathbf{D^3}$ by replacing one of the two CH_3 groups with a hydrogen substituent. Again, self-assembly yielded a complicated NMR spectrum (Supplementary Figs. 130-131), confirming that both methyl groups are crucial for proper self-sorting.

Next, we asked whether similar selective interactions also existed between ligands **A** and **B**. However, ribbon-shaped ligand **A** is actually closer to ligand **D** than to **B** in the X-ray structure

(Fig. 4 left). From a structural point of view, we can only speculate that exactly one count of ligand **A**, possessing a backbone with a spring-like flexibility (Pd-Pd distances in cages containing **A** vary between 13.66 and 15.94 Å), adjusts to the required length in combination with ligands **B**, **C** and **D**, while a pair of **A** leads to a too flexible and a pair of **B** to a too rigid assembly. Indeed, both experimentally obtained values from the reaction of $[Pd_2\mathbf{A}_2\mathbf{CD}]^{4+}$ plus $[Pd_2\mathbf{B}_2\mathbf{CD}]^{4+}$ to give 2x cage $[Pd_2\mathbf{ABCD}]^{4+}$ ($\Delta H = -19.5$ kJ mol^{-1}, $\Delta G = -11.7$ kJ mol^{-1}, see Fig. 5b and van't Hoff analysis in Supplementary Information) as well as the DFT-calculated energy change (ωB97X-D/DEF2-SVP, $\Delta E = -10.1$ kJ mol^{-1}) point to a significant enthalpic driving force for combining ligands **A** and **B** within the same assembly.

To investigate the generality of forming heteroleptic cages with four different components we then screened further ligand variations. First, the replacement of ligand **B** with $\mathbf{B^0}$, containing an N-hexyl carbazole backbone, also resulted in the exclusive formation of a similar cage $[Pd_2\mathbf{AB^0CD}]^{4+}$ (Supplementary Figs. 118-124). X-ray structure analysis revealed that the position of ligands **A**, **C**, and **D** in $[Pd_2\mathbf{AB^0CD}]^{4+}$ almost perfectly overlap with those in $[Pd_2\mathbf{ABCD}]^{4+}$ (Fig. 4b, Supplementary Figs. 298). Given that the dimethyl group on ligand **C** is indispensable to supporting strong enough C-H···π interactions, we then investigated if changing the π-surface of ligand **D** will also have an effect. We found that all ligands $\mathbf{D^1}$, $\mathbf{D^2}$, or $\mathbf{D^3}$ assemble with **A**, **B** and **C** to give clean NMR spectra (Supplementary Figs. 168, 210 and 231). HR-ESI-MS confirmed the formation of corresponding heteroleptic cages with four different ligands. Trapped ion mobility spectrometry (ESI-TIMS-TOF) revealed only one narrow peak for each $[Pd_2\mathbf{ABCD^n}]^{4+}$ cage, supporting the formation of a single isomer (Supplementary Fig. 289). NOESY correlations indicate the formation of the $[Pd_2\mathbf{ABCD^n}]^{4+}$ isomer (n = 1–3) in all cases (Supplementary Figs. 171, 214 and 234). A crystal structure was obtained for cage $[Pd_2\mathbf{ABCD^2}]^{4+}$ and it almost perfectly superimposes with that of cage $[Pd_2\mathbf{ABCD}]^{4+}$ (Supplementary Fig. 298). These results suggest that a wide choice of ligands $\mathbf{D^n}$ with π-surface and suitable length is sufficient to achieve self-sorting.

Next, we tested the combination of naphthalene diimide (NDI) ligand $\mathbf{D^4}$ with **A**, **B**, and **C** and again obtained a well-resolved NMR spectrum, very similar to that of $[Pd_2\mathbf{ABCD}]^{4+}$. HR-ESI-MS confirmed the formula $[2Pd^{II}+\mathbf{A}+\mathbf{B}+\mathbf{C}+\mathbf{D^4}]^{4+}$ (Supplementary Figs. 250-256). We initially expected this species to be the $[Pd_2\mathbf{ABCD^4}]^{4+}$ isomer, however, NOESY indicated a different internal arrangement speaking for a $[Pd_2\mathbf{ABD^4C}]^{4+}$ ligand order by showing correlations between protons H7 of ligand **A** and **C**, and protons H7 of ligand **B** and $\mathbf{D^4}$ (Supplementary Fig. 254). The exclusive formation of a single species was supported by a ^{1}H DOSY experiment (Supplementary Fig. 255). Unambiguous proof for the altered ligand order

in cage $[Pd_2\mathbf{ABD^4C}]^{4+}$ came from X-ray structure analysis (Fig. 4b right). Surprisingly, in contrast to the $[Pd_2\mathbf{ABCD}]^{4+}$ structure where the geminal methyl groups of **C** point to the π-surface of ligand **D**, in $[Pd_2\mathbf{ABD^4C}]^{4+}$, the NDI backbone of ligand **D** rotates in a way that instead of providing its π-surface, two C-H substituents now point to the π-surface of ligand **C** (C-H···π distances 2.82–3.02 Å). The same was observed in the X-ray structure of three-component cage $[Pd_2\mathbf{B}_2\mathbf{D^4C}]^{4+}$ (Fig. 2c).

Concerning the observed ligand order we computed the energies of all three possible isomers for both cages via DFT-based geometry optimizations. Indeed, the experimentally found isomers are also the energetically most favorable ones (Fig. 5a). A reason for the flipped ligand order in $[Pd_2\mathbf{ABCD}]^{4+}$ and $[Pd_2\mathbf{ABD^4C}]^{4+}$ can be deduced from comparing the electron rich/poor character of the directly interacting ligands via their electrostatic surface potential (ESP) maps (Supplementary Fig. 288). While in the former case ligand **C** prefers to make CH_3-π interactions with the π-plane of ligand **D**, in $[Pd_2\mathbf{ABD^4C}]^{4+}$ the methyl groups of **C** refrain to point to the positively polarized NDI-π surface of $\mathbf{D^4}$. Instead, the NDI CH substituents now point towards the π-surface of **C**. This structural flip seems to affect the shape-complementarity with the oppositely arranged ligands, leading to the observed change in ligand order. Finally, we studied the stability difference between both four-component cages by adding ligand **D** to cage $[Pd_2\mathbf{ABD^4C}]^{4+}$ which resulted in quantitative transformation into cage $[Pd_2\mathbf{ABCD}]^{4+}$ (Supplementary Fig. 270). The preferable incorporation of ligand **D** over $\mathbf{D^4}$ was further supported by calculating the ligand exchange via DFT (Fig. 5a).

Evolution of multicomponent heteroleptic cages

The exclusive formation of heteroleptic cages upon mixing of up to four different ligands in solution indicates that all are formed as thermodynamically most stable products. To test whether they can be obtained progressively from their homoleptic or two-component heteroleptic precursors in stepwise cage-to-cage transformations (Fig. 1b), we employed NMR-based mixing experiments, van't Hoff dissection of thermodynamic parameters and DFT computations (Fig. 5b).

Mixing and heating pairs of homoleptic cage solutions ($[Pd_2L_4]$ for **A** and **B**[38,47], mixtures of $[Pd_3L_6]$ rings and $[Pd_4L_8]$ tetrahedra for **C** and **D**[42,46]; 1:1 stoichiometry with respect to ligand count) led to the clean transformation into two-component cages $[Pd_2\mathbf{A}_2\mathbf{C}_2]^{4+}$, $[Pd_2\mathbf{A}_2\mathbf{D}_2]^{4+}$, $[Pd_2\mathbf{B}_2\mathbf{C}_2]^{4+}$, and $[Pd_2\mathbf{B}_2\mathbf{D}_2]^{4+}$ (going from level I to II in Fig. 1b and Supplementary Fig. 257). Further, mixing pairs of these two-component cages allowed to obtain three-component cages $[Pd_2\mathbf{A}_2\mathbf{CD}]^{4+}$, $[Pd_2\mathbf{ABC}_2]^{4+}$, $[Pd_2\mathbf{ABD}_2]^{4+}$ and $[Pd_2\mathbf{B}_2\mathbf{CD}]^{4+}$ (level II to III in Fig. 1b and

Supplementary Figs. 272-279). Finally, cage $[Pd_2\mathbf{ABCD}]^{4+}$ could be obtained by either combining two-component cages $[Pd_2\mathbf{A}_2\mathbf{C}_2]^{4+}$ with $[Pd_2\mathbf{B}_2\mathbf{D}_2]^{4+}$ or $[Pd_2\mathbf{A}_2\mathbf{D}_2]^{4+}$ with $[Pd_2\mathbf{B}_2\mathbf{C}_2]^{4+}$ (level II to IV in Fig. 1b and Supplementary Figs. 284-287) or three-component cages $[Pd_2\mathbf{A}_2\mathbf{CD}]^{4+}$ with $[Pd_2\mathbf{B}_2\mathbf{CD}]^{4+}$ or $[Pd_2\mathbf{ABC}_2]^{4+}$ with $[Pd_2\mathbf{ABD}_2]^{4+}$ (level III to IV in Fig. 1b and Supplementary Figs. 280-283). Besides these stepwise procedures, it is also possible to form cage $[Pd_2\mathbf{ABCD}]^{4+}$ directly by mixing all four homoleptic assemblies (level I to IV; *route v* in Fig. 1b and Supplementary Fig. 268).

For two routes, both starting from level II, we determined the Gibbs free energy changes for all cage-to-cage transformations by NMR-based equilibrium constant calculation (Fig. 5b) and further dissected the thermodynamic parameters by van't Hoff analyses, confirming that each step (from level II to III to IV) is energetically downhill. Notably, almost identical summed-up ΔG^{353K} values (–54.8 kJ/mol and –52.1 kJ/mol) were calculated for both routes towards cage $[Pd_2\mathbf{ABCD}]^{4+}$ (Supplementary Fig. 286, Supplementary Table 2). In addition, kinetic data was obtained for a selection of cage-to-cage transformations by time-dependent NMR measurements, revealing that conversions from level II to III are faster when ligand **A** is contained instead of **B** (e.g $[Pd_2\mathbf{A}_2\mathbf{C}_2]^{4+} + [Pd_2\mathbf{A}_2\mathbf{D}_2]^{4+} \rightarrow 2\ [Pd_2\mathbf{A}_2\mathbf{CD}]^{4+}$: $t_{½}$ = 17.9 min vs. $[Pd_2\mathbf{B}_2\mathbf{C}_2]^{4+} + [Pd_2\mathbf{B}_2\mathbf{D}_2]^{4+} \rightarrow 2\ [Pd_2\mathbf{B}_2\mathbf{CD}]^{4+}$: $t_{½}$ = 41.5 min), which may again be explained by the higher structural flexibility of ligand **A**, facilitating ligand exchange from/to the square-planar Pd^{II} centers in the constrained 3D assembly. To rule out electronic influences, we compared structurally similar ligands **B** (electron-poor) and $\mathbf{B^0}$ (electron-rich) and found virtually the same conversion kinetics, further supporting our assumption (Supplementary Figs. 258-267, Supplementary Table 1).

Conclusion

A carefully chosen set of four different bis-monodentate ligands (**A**, **B**, **C** and **D**), all carrying the same kind of pyridyl donor groups, assembles with Pd^{II} cations to a single nanoscopic cage $[Pd_2\mathbf{ABCD}]^{4+}$ in a non-statistical fashion. Key for achieving this high degree of integrative self-sorting is the combination of ligand shape complementarity, balance of strain and interligand C-H···π interactions. The modular replacement of ligands, even allowing to control their order around the metals, paves the way for further derivatization to embed functionality. As the assembly proceeds under full thermodynamic control, formed products are robust and produced in a reproducible manner, following several alternative routes. The rational self-assembly strategy allows to maximize the degree of ligand differentiation within the Pd^{II}-cage

family with the lowest nuclearity, selectively yielding one out of 55 possible products. As a general concept, this enables the development of multifunctional assemblies in which the interplay of different components leads to emerging properties, attractive for applications in selective recognition, cooperative catalysis and materials science.

Acknowledgments

We thank the European Research Council (ERC Consolidator grant 683083, RAMSES) for financial support. This work was funded by the Deutsche Forschungsgemeinschaft (DFG, German Research Foundation) under Germany's Excellence Strategy EXC 2033 “RESOLV”, project number 390677874, and GRK2376 “Confinement-controlled Chemistry”, project number 331085229. The authors thank Dr. Bin Chen, Dr. Jacopo Tessarolo, André Platzek, Kristina Ebbert and Dr. Shota Hasegawa for providing ligands and Laura Schneider for ESI mass spectra measurements. We thank Dr. Julian J. Holstein for helpful suggestions on the crystallographic data analysis.

Author contributions

K.W. and G.H.C conceived the project and wrote the manuscript together with E.B. K.W. performed the experiments and analyzed the data. A.B. provided ion-mobility mass measurements. K.W. collected the X-ray single-crystal data and refined the crystal structures.

Competing Interests

The authors declare no competing interests.

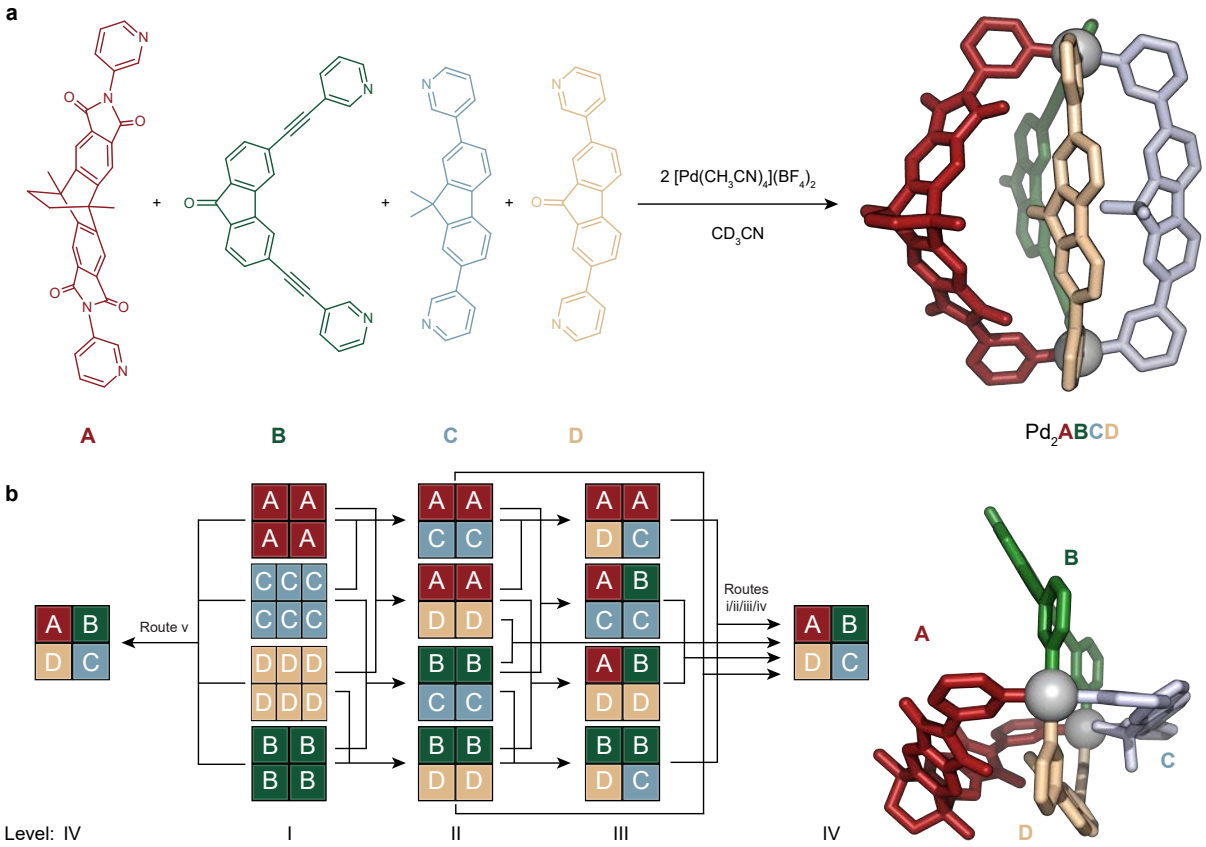

Fig. 1 | Self-assembly of heteroleptic multicomponent cage $[Pd_2ABCD]^{4+}$ from four chemically different ligands. a, cage formation from ligands **A**, **B**, **C**, **D** and Pd^{II} (X-ray structure of $[Pd_2\mathbf{ABCD}]^{4+}$ depicted as side and top view). **b,** Evolution of complexity from homoleptic assemblies to the most complex heteroleptic assembly $[Pd_2\mathbf{ABCD}]^{4+}$ via different pathways.

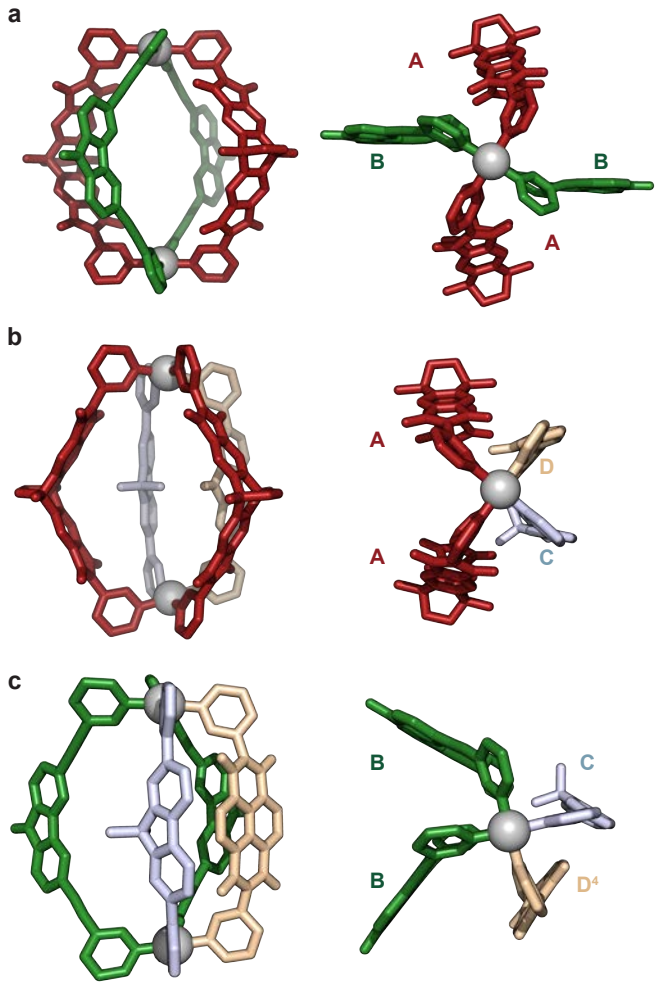

Fig. 2 | X-ray crystal structures of multicomponent heteroleptic cages with two or three different ligands. Side and top views of **a**, *trans*-$[Pd_2\mathbf{A}_2\mathbf{B}_2]^{4+}$; **b**, $[Pd_2\mathbf{A}_2\mathbf{CD}]^{4+}$ and **c**, $[Pd_2\mathbf{B}_2\mathbf{D}^4\mathbf{C}]^{4+}$ (counter anions, solvents and hydrogens omitted for clarity, further details see Supplementary Information). In **b**, the dihedral angle between the two $[Pd(Py)_4]$ planes in the structure is 33.9°, indicating the presence of pronounced shape-complementarity, with **A** being the longer ligand opposite two shorter ligands **C** and $\mathbf{D}^{33}$.

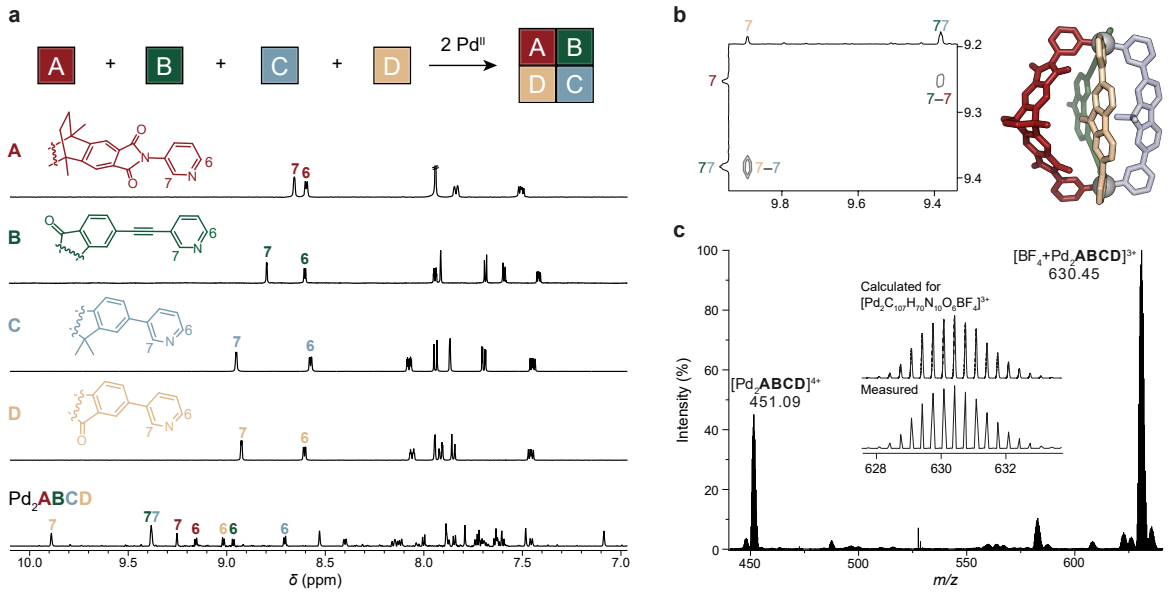

Fig. 3 | Characterization of heteroleptic multicomponent cage $[Pd_2ABCD]^{4+}$. a, From top to bottom, ^1H NMR spectra (700 MHz, 298 K, CD_3CN) of **A**, **B**, **C**, **D**, $[Pd_2\mathbf{ABCD}]^{4+}$. **b,** Partial ^1H–^1H NOESY spectrum of $[Pd_2\mathbf{ABCD}]^{4+}$, revealing correlations between protons H7 of two ligand pairs. **c,** HR-ESI-MS of $[Pd_2\mathbf{ABCD}]^{4+}$ (isotopic pattern shown as inset).

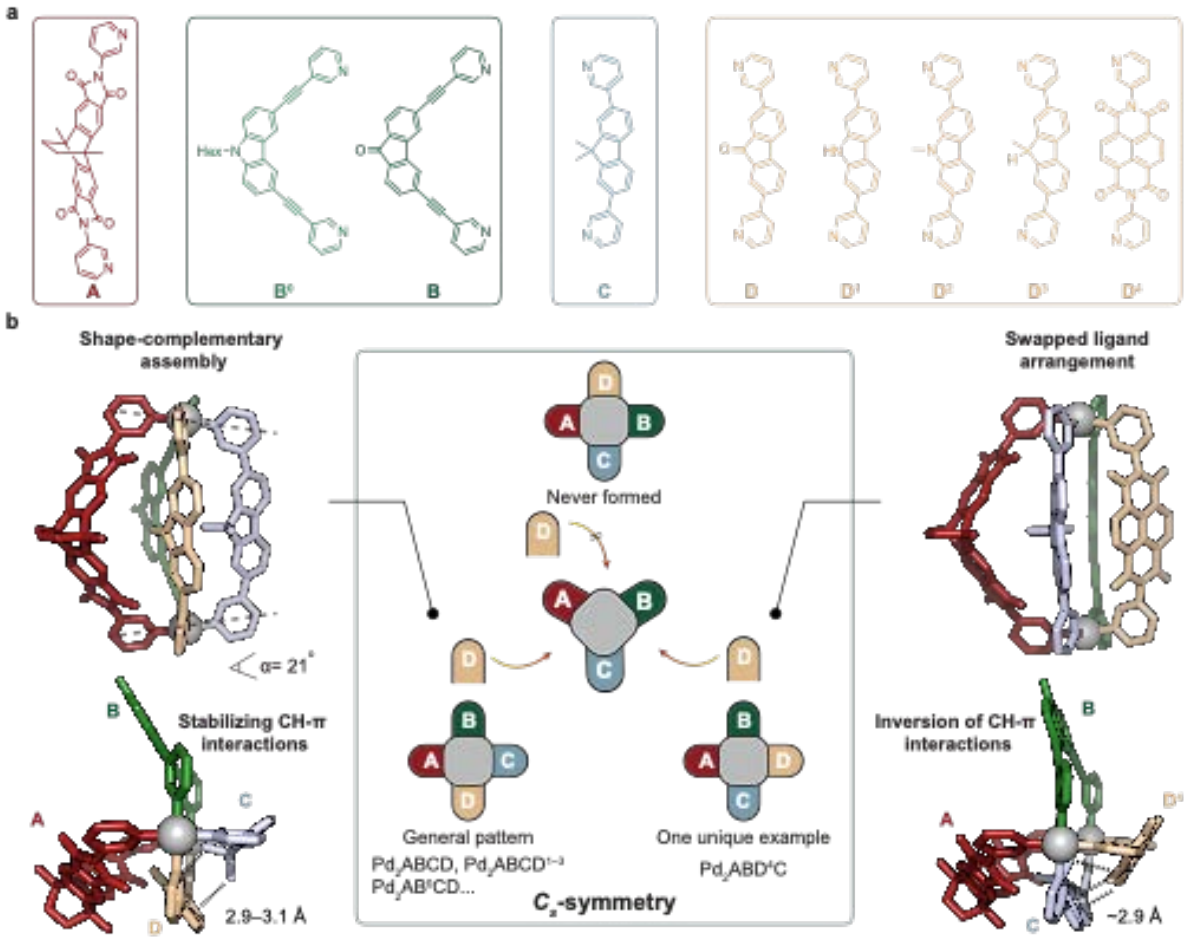

Fig. 4 | Possible cage isomers and comparison of crystal structures of [Pd$_2$ABCD] and [Pd$_2$ABD^{4}C]. **a,** Used ligands. **b,** Left: side and top X-ray views of cage [Pd$_2$**ABCD**]$^{4+}$ (dihedral angle ∠α between [Pd(Py)$_4$] planes indicates the presence of pronounced shape-complementarity; distances of C-H···π interactions between **C** and **D** are given). All ligand combinations with **D**, and **D^1**–**D^3** led to the general **ABCD** pattern. Middle: All three configurational isomers with C_s-symmetry obtained by arranging four different ligands circularly around two metal nodes are shown. Right: side and top X-ray views of [Pd$_2$**ABD^{4}C**] showing a swapped ligand arrangement and inversion of C-H···π interactions (C-H···π distance between ligands **D^4** and **C** given).

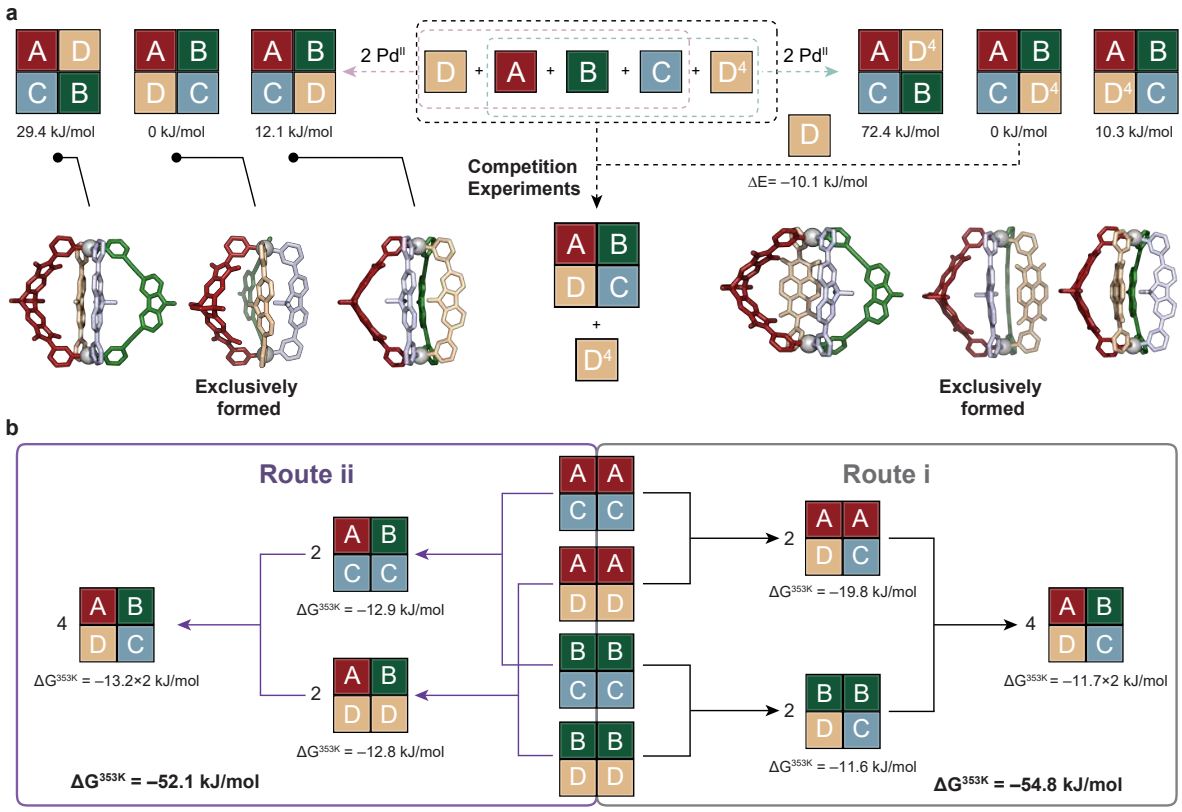

Fig. 5 | Thermodynamic analysis of cage isomers, competition experiments and sequential formation of [Pd$_2$ABCD]. **a,** Relative DFT-calculated energies and geometry-optimized structures of the three possible isomers formed from **A**, **B**, **C** plus **D** or **D^4**. Competition experiments showing preferential formation of [Pd$_2$**ABCD**]$^{4+}$ over [Pd$_2$**ABD^{4}C**]$^{4+}$ and calculated energetic difference. **b,** Formation of [Pd$_2$**ABCD**]$^{4+}$ via two different routes and measured free energy changes for each step.

References

1. Kelly, J. A., Sielecki, A. R., Sykes, B. D., James, M. N. G. & Phillips, D. C. X-ray crystallography of the binding of the bacterial cell wall trisaccharide NAM-NAG-NAM to lysozyme. *Nature* **282**, 875–878 (1979).
2. Ringe, D. & Petsko, G. A. How Enzymes Work. *Science* **320**, 1428–1429 (2008).

3. Liu, M. et al. Barely porous organic cages for hydrogen isotope separation. *Science* **366**, 613–620 (2019).
4. Cook, T. R. & Stang, P. J. Recent Developments in the Preparation and Chemistry of Metallacycles and Metallacages via Coordination. *Chem. Rev.* **115**, 7001–7045 (2015).
5. Fujita, M. et al. Self-assembly of ten molecules into nanometre-sized organic host frameworks. *Nature* **378**, 469–471 (1995).
6. Mal, P., Breiner, B., Rissanen, K. & Nitschke, J. R. White Phosphorus Is Air-Stable Within a Self-Assembled Tetrahedral Capsule. *Science* **324**, 1697–1699 (2009).
7. Zhang, D., Ronson, T. K., Zou, Y.-Q. & Nitschke, J. R. Metal–organic cages for molecular separations. *Nat. Rev. Chem.* **5**, 168–182 (2021).
8. Galan, A. & Ballester, P. Stabilization of reactive species by supramolecular encapsulation. *Chem. Soc. Rev.* **45**, 1720–1737 (2016).
9. Brown, C. J., Toste, F. D., Bergman, R. G. & Raymond, K. N. Supramolecular Catalysis in Metal–Ligand Cluster Hosts. *Chem. Rev.* **115**, 3012–3035 (2015).
10. Chen, L.-J., Yang, H.-B. & Shionoya, M. Chiral metallosupramolecular architectures. *Chem. Soc. Rev.* **46**, 2555–2576 (2017).
11. Brzechwa-Chodzyńska, A., Drożdż, W., Harrowfield, J. & Stefankiewicz, A. R. Fluorescent sensors: A bright future for cages. *Coord. Chem. Rev.* **434**, 213820 (2021).
12. Goeb, S. & Sallé, M. Electron-rich Coordination Receptors Based on Tetrathiafulvalene Derivatives: Controlling the Host–Guest Binding. *Acc. Chem. Res.* **54**, 1043–1055 (2021).
13. Wu, K. et al. The Redox Coupling Effect in a Photocatalytic Ru^{II}-Pd^{II} Cage with TTF Guest as Electron Relay Mediator for Visible-Light Hydrogen-Evolving Promotion. *Angew. Chem. Int. Ed.* **59**, 2639–2643 (2020).
14. Wezenberg, S. J. Light-switchable Metal-Organic Cages. *Chem. Lett.* **49**, 609–615 (2020).
15. Li, R.-J., Tessarolo, J., Lee, H. & Clever, G. H. Multi-stimuli Control over Assembly and Guest Binding in Metallo-supramolecular Hosts Based on Dithienylethene Photoswitches. *J. Am. Chem. Soc.* **143**, 3865–3873 (2021).
16. Chakrabarty, R., Mukherjee, P. S. & Stang, P. J. Supramolecular Coordination: Self-Assembly of Finite Two- and Three-Dimensional Ensembles. *Chem. Rev.* **111**, 6810–6918 (2011).
17. Fujita, D. et al. Self-assembly of tetravalent Goldberg polyhedra from 144 small components. *Nature* **540**, 563–566 (2016).
18. Wu, K., Tessarolo, J., Baksi, A. & Clever, G. H. Guest-Modulated Circularly Polarized Luminescence by Ligand-to-Ligand Chirality Transfer in Heteroleptic PdII Coordination Cages. *Angew. Chem. Int. Ed.* **61**, e202205725 (2022).
19. Frank, M. et al. Light-Induced Charge Separation in Densely Packed Donor–Acceptor Coordination Cages. *J. Am. Chem. Soc.* **138**, 8279–8287 (2016).
20. García-Simón, C. et al. Enantioselective Hydroformylation by a Rh-Catalyst Entrapped in a Supramolecular Metallocage. *J. Am. Chem. Soc.* **137**, 2680–2687 (2015).
21. Wang, Q.-Q. et al. Self-assembled nanospheres with multiple endohedral binding sites pre-organize catalysts and substrates for highly efficient reactions. *Nat. Chem.* **8**, 225–230 (2016).
22. Howlader, P., Das, P., Zangrando, E. & Mukherjee, P. S. Urea-Functionalized Self-Assembled Molecular Prism for Heterogeneous Catalysis in Water. *J. Am. Chem. Soc.* **138**, 1668–1676 (2016).
23. Pruchyathamkorn, J. et al. A Complex Comprising a Cyanine Dye Rotaxane and a Porphyrin Nanoring as a Model Light-Harvesting System. *Angew. Chem. Int. Ed.* **59**, 16455–16458 (2020).

24. Wang, W. et al. The construction of complex multicomponent supramolecular systems via the combination of orthogonal self-assembly and the self-sorting approach. *Chem. Sci.* **5**, 4554–4560 (2014).
25. Kramer, R., Lehn, J. M. & Marquis-Rigault, A. Self-recognition in helicate self-assembly: spontaneous formation of helical metal complexes from mixtures of ligands and metal ions. *Proc. Natl. Acad. Sci. USA* **90**, 5394–5398 (1993).
26. Sauvage, J. P. & Weiss, J. Synthesis of biscopper(I) [3]-catenates: multiring interlocked coordinating systems. *J. Am. Chem. Soc.* **107**, 6108–6110 (1985).
27. Kumazawa, K., Biradha, K., Kusukawa, T., Okano, T. & Fujita, M. Multicomponent Assembly of a Pyrazine-Pillared Coordination Cage That Selectively Binds Planar Guests by Intercalation. *Angew. Chem. Int. Ed.* **42**, 3909–3913 (2003).
28. Zheng, Y.-R. et al. A Facile Approach toward Multicomponent Supramolecular Structures: Selective Self-Assembly via Charge Separation. *J. Am. Chem. Soc.* **132**, 16873–16882 (2010).
29. Wessjohann, L. A., Kreye, O. & Rivera, D. G. One-Pot Assembly of Amino Acid Bridged Hybrid Macromulticyclic Cages through Multiple Multicomponent Macrocyclizations. *Angew. Chem. Int. Ed.* **56**, 3501–3505 (2017).
30. He, Z., Jiang, W. & Schalley, C. A. Integrative self-sorting: a versatile strategy for the construction of complex supramolecular architecture. *Chem. Soc. Rev.* **44**, 779–789 (2015).
31. Pullen, S., Tessarolo, J. & Clever, G. H. Increasing structural and functional complexity in self-assembled coordination cages. *Chem. Sci.* **12**, 7269–7293 (2021).
32. Sun, Q.-F., Sato, S. & Fujita, M. An $M_{12}(L^1)_{12}(L^2)_{12}$ Cantellated Tetrahedron: A Case Study on Mixed-Ligand Self-Assembly. *Angew. Chem. Int. Ed.* **53**, 13510–13513 (2014).
33. Bloch, W. M. et al. Geometric Complementarity in Assembly and Guest Recognition of a Bent Heteroleptic *cis*-$[Pd_2L^A_2L^B_2]$ Coordination Cage. *J. Am. Chem. Soc.* **138**, 13750–13755 (2016).
34. Sudan, S. et al. Identification of a Heteroleptic $Pd_6L_6L'_6$ Coordination Cage by Screening of a Virtual Combinatorial Library. *J. Am. Chem. Soc.* **143**, 1773–1778 (2021).
35. Li, J.-R. & Zhou, H.-C. Bridging-ligand-substitution strategy for the preparation of metal–organic polyhedra. *Nat. Chem.* **2**, 893–898 (2010).
36. Prusty, S., Yazaki, K., Yoshizawa, M. & Chand, D. K. A Truncated Molecular Star. *Chem. Eur. J.* **23**, 12456–12461 (2017).
37. Yamashina, M., Yuki, T., Sei, Y., Akita, M. & Yoshizawa, M. Anisotropic Expansion of an M_2L_4 Coordination Capsule: Host Capability and Frame Rearrangement. *Chem. Eur. J.* **21**, 4200–4204 (2015).
38. Chen, B., Holstein, J. J., Horiuchi, S., Hiller, W. G. & Clever, G. H. Pd(II) Coordination Sphere Engineering: Pyridine Cages, Quinoline Bowls, and Heteroleptic Pills Binding One or Two Fullerenes. *J. Am. Chem. Soc.* **141**, 8907–8913 (2019).
39. Preston, D., Barnsley, J. E., Gordon, K. C. & Crowley, J. D. Controlled Formation of Heteroleptic $[Pd_2(L_a)_2(L_b)_2]^{4+}$ Cages. *J. Am. Chem. Soc.* **138**, 10578–10585 (2016).
40. Ogata, D. & Yuasa, J. Dynamic Open Coordination Cage from Nonsymmetrical Imidazole–Pyridine Ditopic Ligands for Turn-On/Off Anion Binding. *Angew. Chem. Int. Ed.* **58**, 18424–18428 (2019).
41. Lewis, J. E. M., Tarzia, A., White, A. J. P. & Jelfs, K. E. Conformational control of Pd_2L_4 assemblies with unsymmetrical ligands. *Chem. Sci.* **11**, 677–683 (2020).

42. Tessarolo, J., Lee, H., Sakuda, E., Umakoshi, K. & Clever, G. H. Integrative Assembly of Heteroleptic Tetrahedra Controlled by Backbone Steric Bulk. *J. Am. Chem. Soc.* **143**, 6339–6344 (2021).
43. De, S., Mahata, K. & Schmittel, M. Metal-coordination-driven dynamic heteroleptic architectures. *Chem. Soc. Rev.* **39**, 1555–1575 (2010).
44. Johnson, A. M. & Hooley, R. J. Steric Effects Control Self-Sorting in Self-Assembled Clusters. *Inorg. Chem.* **50**, 4671–4673 (2011).
45. Liu, Y. et al. Controlled Construction of Heteroleptic $[Pd_2(L^A)_2(L^B)(L^C)]^{4+}$ Cages: A Facile Approach for Site-Selective endo-Functionalization of Supramolecular Cavities. *Angew. Chem. Int. Ed.* **62**, e202217215 (2023).
46. Wu, K., Zhang, B., Drechsler, C., Holstein, J. J. & Clever, G. H. Backbone-Bridging Promotes Diversity in Heteroleptic Cages. *Angew. Chem. Int. Ed.* **60**, 6403–6407 (2021).
47. Ebbert, K. E. et al. Resolution of minor size differences in a family of heteroleptic coordination cages by trapped ion mobility ESI-MS. *Dalton Trans.* **48**, 11070–11075 (2019).

Methods

Exemplary synthetic protocols, analytical data listings and interpretation:

Self-assembly of two-component cage $[Pd_2B_2C_2](BF_4)_4$.

To a solution of **C** (120 µL, 3 mM, 0.36 µmol) and a suspension of **B** (120 µL, 3 mM, 0.36 µmol) in CD_3CN were added a stock solution of $[Pd(CH_3CN)_4](BF_4)_2$ (24 µL, 15 mM/CD_3CN, 0.36 µmol) and 186 µL CD_3CN. The mixture was heated in an NMR tube at 80 °C for 8 h to give a 0.4 mM cage solution.

^{1}H NMR (500 MHz, 298 K, CD_3CN) δ 9.55 (d, *J* = 2.0 Hz, 4H), 9.43 (d, *J* = 1.8 Hz, 4H), 9.12 (dd, *J* = 5.9, 1.4 Hz, 4H), 9.02 (d, *J* = 5.8 Hz, 4H), 8.25 – 8.21 (m, 4H), 8.18 (dt, *J* = 8.1, 1.6 Hz, 4H), 7.95 (d, *J* = 7.7 Hz, 4H), 7.77 (s, 4H), 7.72 – 7.64 (m, 16H), 7.57 (d, *J* = 1.7 Hz, 4H), 7.49 (dd, *J* = 7.8, 1.7 Hz, 4H), 1.63 (s, 6H), 1.29 (s, 6H).

^{13}C NMR (176 MHz, 298 K, CD_3CN) δ 192.17, 156.86, 153.88, 151.25, 150.58, 150.16, 144.76, 144.73, 143.14, 140.66, 139.71, 136.11, 135.99, 135.52, 128.95, 128.87, 128.44, 128.31, 125.24, 124.25, 123.74, 122.93, 122.70, 95.43, 87.58, 48.26, 29.84, 25.86.

HR-ESI-MS $[BF_4{+}Pd_2\mathbf{B_2C_2}]^{3+}$: *m/z* measured: 587.1211, calculated: 587.1200.

Self-assembly of three-component cage $[Pd_2A_2CD](BF_4)_4$.

To a solution of **A** (120 µL, 3 mM, 0.36 µmol), **C** (60 µL, 3 mM, 0.18 µmol) and a suspension of **D** (60 µL, 3 mM, 0.18 µmol) in CD_3CN were added a stock solution of $[Pd(CH_3CN)_4](BF_4)_2$ (24 µL, 15 mM/CD_3CN, 0.36 µmol) and 186 µL CD_3CN. The mixture was heated at 80 °C for 8 h to give a 0.4 mM cage solution.

^{1}H NMR (700 MHz, 298 K, CD_3CN) δ 9.73 (d, J = 2.1 Hz, 2H), 9.36 (d, J = 2.2 Hz, 2H), 9.24 (d, J = 2.0 Hz, 2H), 9.03 (dd, J = 6.1, 1.3 Hz, 2H), 9.00 (dd, J = 6.0, 1.2 Hz, 2H), 8.98 (d, J = 2.2 Hz, 2H), 8.87 (dd, J = 6.0, 1.2 Hz, 2H), 8.78 (dd, J = 5.9, 1.3 Hz, 2H), 8.36 (ddd, J = 7.9, 2.0, 1.3 Hz, 2H), 8.35 – 8.33 (m, 2H), 8.23 (ddd, J = 8.2, 2.2, 1.2 Hz, 2H), 8.15 – 8.12 (m, 2H), 8.05 – 8.01 (m, 4H), 7.93 (dd, J = 7.6, 0.6 Hz, 2H), 7.83 – 7.78 (m, 8H), 7.74 (s, 2H), 7.72 (s, 2H), 7.71 – 7.68 (m, 2H), 7.61 – 7.60 (m, 2H), 7.59 – 7.56 (m, 2H), 7.51 (dd, J = 7.7, 1.8 Hz, 2H), 6.99 (d, J = 1.8 Hz, 2H), 2.28 (s, 3H), 2.08 (s, 3H), 2.05 (s, 3H), 1.93 (s, 3H), 1.76 – 1.72 (m, 8H), 0.91 (s, 3H), 0.44 (s, 3H).

^{13}C NMR (176 MHz, 298 K, CD_3CN) δ 192.83, 172.98, 167.61, 167.12, 166.90, 166.79, 166.74, 166.61, 155.76, 154.75, 154.58, 154.52, 154.37, 154.27, 154.19, 151.36, 150.62, 150.45, 150.34, 150.22, 150.05, 149.91, 149.32, 145.82, 142.33, 140.09, 139.88, 139.79, 139.45, 139.17, 138.60, 138.41, 136.97, 136.79, 135.57, 132.05, 131.68, 130.64, 130.45, 128.73, 128.50, 128.25, 127.88, 124.68, 123.33, 123.10, 122.13, 117.56, 117.52, 46.64, 45.59, 45.35, 45.14, 44.98, 35.00, 34.83, 34.76, 34.69, 34.48, 30.36, 30.30, 30.07, 29.99, 29.77.

2D NMR spectra were employed to assign all signals unambiguously and the correlation between proton H7 on ligand **C** (blue) and H7 on ligand **D** (yellow) allowed us to confirm the formation of a *cis*-configured $[Pd_2\mathbf{A}_2\mathbf{CD}]^{4+}$ cage (Supplementary Figs. 67-68). In the cage, both ligands **A** adjacent to **C** and **D** are not equivalent anymore, resulting in two sets of NMR signals.

HR-ESI-MS provided convincing evidence for the expected stoichiometry by showing a series of peaks assigned to $[2Pd^{II}+2\mathbf{A}+\mathbf{C}+\mathbf{D}+nBF_4]^{(4-n)+}$ (n = 0–2; Supplementary Fig. 70).

Self-assembly of tetra-component cage $[Pd_2ABCD](BF_4)_4$.

To a solution of **A** (60 μL, 3 mM, 0.18 μmol), **C** (60 μL, 3 mM, 0.18 μmol) and a suspension of **B** (60 μL, 3 mM, 0.18 μmol), **D** (60 μL, 3 mM, 0.18 μmol) were added a stock solution of $[Pd(CH_3CN)_4](BF_4)_2$ (24 μL, 15 mM/CD_3CN, 0.36 μmol) and 186 μL CD_3CN. The mixture was heated in an NMR tube at 80 °C for 8 h to give a 0.4 mM cage solution.

^{1}H NMR (700 MHz, 298 K, CD_3CN) δ 9.89 (d, *J* = 2.1 Hz, 2H), 9.38 (t, *J* = 2.7 Hz, 4H), 9.25 (d, *J* = 1.9 Hz, 2H), 9.16 (d, *J* = 5.9 Hz, 2H), 9.02 (d, *J* = 5.8 Hz, 2H), 8.97 (d, *J* = 5.8 Hz, 2H), 8.71 (d, *J* = 6.0 Hz, 2H), 8.53 (d, *J* = 1.8 Hz, 2H), 8.40 (d, *J* = 7.8 Hz, 2H), 8.17 – 8.10 (m, 4H), 8.00 (d, *J* = 7.5 Hz, 2H), 7.90 – 7.86 (m, 4H), 7.85 (d, *J* = 7.7 Hz, 2H), 7.79 (s, 2H), 7.75 – 7.69 (m, 6H), 7.65 – 7.61 (m, 4H), 7.61 – 7.59 (m, 2H), 7.48 (s, 2H), 7.46 (dd, *J* = 7.6, 1.8 Hz, 2H), 7.09 (d, *J* = 1.8 Hz, 2H), 2.12 (s, 3H), 1.97 (s, 3H), 1.81 (s, 4H), 1.32 (s, 3H), 0.55 (s, 3H).

^{13}C NMR (151 MHz, 298 K, CD_3CN) δ 194.28, 192.81, 173.03, 167.76, 167.65, 167.11, 166.94, 154.71, 154.63, 153.97, 151.26, 151.15, 150.50, 150.43, 150.32, 149.86, 149.83,

145.99, 144.74, 142.35, 142.03, 140.18, 139.66, 139.08, 138.48, 138.42, 137.29, 136.69, 136.23, 135.69, 135.46, 131.86, 130.66, 130.58, 128.69, 128.49, 128.38, 128.34, 127.92, 125.13, 124.89, 124.07, 123.64, 123.44, 123.05, 122.69, 117.56, 95.28, 87.38, 46.85, 45.04, 32.64, 30.37, 27.10, 23.39, 18.75, 14.39.

HR-ESI-MS $[BF_4+Pd_2\mathbf{ABCD}]^{3+}$: *m/z* measured: 630.4541, calculated: 630.4539.

Single crystal X-ray analysis shows that the cage crystallizes in the $P\bar{1}$ space group, with the asymmetric unit containing one cage molecule. The Pd···Pd distance in the structure is 13.67 Å, comparable to that found in the $[Pd_2\mathbf{A}_2\mathbf{CD}]^{4+}$ structure (14.33 Å).

Data availability statement

Crystallographic data for the structures reported in this paper have been deposited at the Cambridge Crystallographic Data Centre, under the deposition numbers 2207621 *trans*-$[Pd_2\mathbf{A}_2\mathbf{B}_2](BF_4)_4$, 2285849 $[Pd_2\mathbf{B}_2\mathbf{CD}^{\mathbf{1}}](BF_4)_4$, 2207623 $[Pd_2\mathbf{A}_2\mathbf{CD}](BF_4)_4$, 2285847 $[Pd_2\mathbf{B}_2\mathbf{D}^{\mathbf{4}}\mathbf{C}](BF_4)_4$, 2285846 $[Pd_2\mathbf{ABCD}](BF_4)_4$, 2207626 $[Pd_2\mathbf{AB}^{\mathbf{0}}\mathbf{CD}](BF_4)_4$, 2207627 $[Pd_2\mathbf{ABD}^{\mathbf{4}}\mathbf{C}](BF_4)_4$, 2207628 $[Pd_2\mathbf{ABD}^{\mathbf{2}}\mathbf{D}](BF_4)_4$, 2285848 $[Pd_2\mathbf{ABCD}^{\mathbf{2}}](BF_4)_4$. Copies of these data can be obtained free of charge via www.ccdc.cam.ac.uk/data_request/cif. All other data supporting the findings of this study are available within the Article and its Supplementary Information, or from the corresponding author upon reasonable request.